Received 7 May 2020; revised 7 July 2020; accepted 8 July 2020. Date of publication 13 July 2020; date of current version 30 July 2020.
The review of this article was arranged by Editor K. Shenai.

Digital Object Identifier 10.1109/JEDS.2020.3008816

Mechanism of AlGaAs/InGaAs pHEMT Nonlinear Response Under High-Power Microwave Radiation

YU-QIAN LIU [1], CHANG-CHUN CHAI [1], HAN WU [1], YU-HANG ZHANG [2], CHUN-LEI SHI [3], AND YIN-TANG YANG [1] (Senior Member, IEEE)

1 Key Laboratory of Ministry of Education for Wide Band-Gap Semiconductor Materials and Devices, School of Microelectronics, Xidian University, Xi'an 710071, China
2 Department of Micro-Nano Electronics, Shanghai Jiao Tong University, Shanghai 200240, China
3 School of Airworthiness, Civil Aviation University of China, Tianjin 300300, China

CORRESPONDING AUTHOR: Y.-Q. LIU (e-mail: yuqianliuxd@163.com)

This work was supported by the National Natural Science Foundation of China 61974116.

ABSTRACT With the development of microelectronic technology, the reliability of devices in a complex electromagnetic environment has become one of the greatest challenges in the semiconductor industry. On this basis, a phenomenon of nonlinear transient response is observed in high-power microwave (HPM)-radiating AlGaAs/InGaAs pseudomorphic high-electron-mobility transistors (pHEMTs). This abnormal response is induced before the thermal failure, causing disturbances to the circuit. To understand this phenomenon, a detailed mechanism analysis is proposed. The analysis shows that the nonlinear response is initially associated with the 2DEG velocity saturation, then a breakdown process is induced by the tunneling and impact ionization combined effect. Within each radiation period, the channel current changes its direction twice under the influence of the HPM field. The nonlinear response current I_d is derived from the theoretical analysis. TCAD simulations demonstrate the saturation and breakdown process. Corresponding experiments are performed using a Ka-band low-noise amplifier (LNA) chip. The results support the theory well.

INDEX TERMS High-power microwave (HPM), pHEMT, nonlinear response, mechanism.

I. INTRODUCTION

The III-V compound semiconductors have been believed to be one of the most promising candidates for radio-frequency (RF) applications and are expected to be next-generation microelectronics beyond Moore's Law [1]–[4]. GaAs-based pseudomorphic high-electron-mobility transistors (pHEMTs) are currently widely used. Their natural advantages of high electron mobility, high quantum efficiency, and high switching speed are exploited in RF low-noise amplifiers (LNAs) and power amplifiers (PAs) [5]–[8].

As the core components of the RF front-end circuits, pHEMT low-noise amplifiers (LNAs) and power amplifiers (PAs) are vulnerable to high-power microwave (HPM) interference [9]–[11]. Much attention has been paid to achieving better performance of high-electron-mobility transistor (HEMT) devices [12]–[17]. Regarding the associated HPM reliability, previous studies, including experimental findings and theoretical explanations, focus primarily on the thermal damage [18]–[23]. When the HEMT is exposed to HPM radiation, the device output is disturbed nonlinearly before burnout [24]. This phenomenon of nonlinear response is more easily induced and has brought complicated disturbances to the circuit. Furthermore, the failure diagnosis and location are challenging in the nonlinearly disturbed circuits because no physical damage can be observed in the device. Therefore, it is essential to understand the mechanism of the HPM induced nonlinear transient response.

In this paper, we attempt to provide a complete physical mechanism analysis of the AlGaAs/InGaAs pHEMT nonlinear transient response under HPM radiation. The "rise – stable – re-rise" response of the device subjected to interference is revealed. Mechanisms of electron velocity

This work is licensed under a Creative Commons Attribution 4.0 License. For more information, see https://creativecommons.org/licenses/by/4.0/

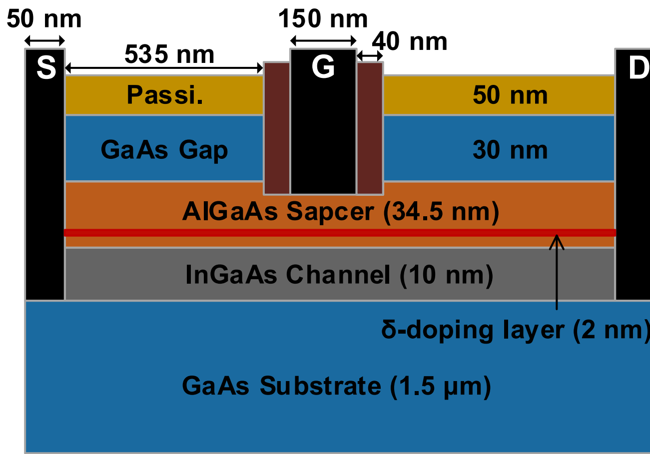

FIGURE 1. The device structure of the AlGaAs/InGaAs pHEMT.

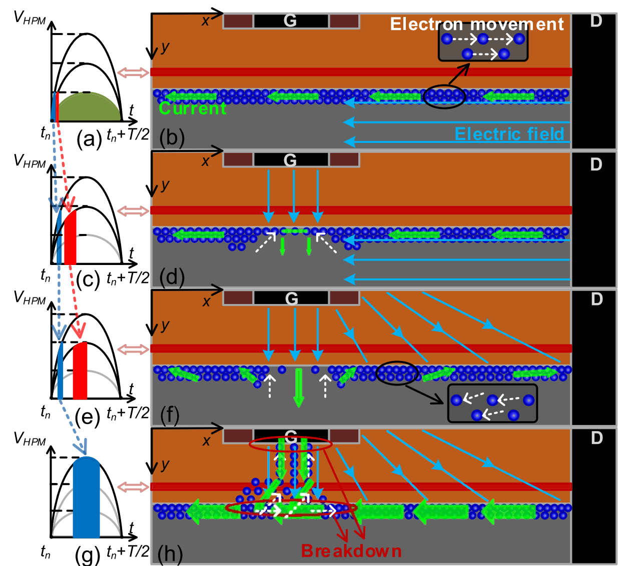

FIGURE 2. Mechanism of the nonlinear response process in the HPM affected pHEMT. (a), (c), (e), and (g) plot the HPM radiation conditions; the corresponding internal states of the device local are shown in (b), (d), (f), and (h).

saturation, tunneling, and impact ionization are utilized to explain the different stages of the nonlinear process. Corresponding experiments are carried out. Relevant simulation is accomplished by Sentaurus TCAD [25], the results confirm our mechanism investigation. Circuit disorders induced by the nonlinear transient response and feasible reinforcement methods are discussed based on pHEMT LNAs. This study can help raise the radiation robustness of GaAs pHEMT-based PAs and LNAs. And it is hoped that the analysis approach promotes the HPM reliability research on other III-V compound semiconductor devices.

II. MECHANISM ANALYSIS OF THE NONLINEAR RESPONSE

A. DEVICE STRUCTURE AND SETUP

Fig. 1 shows the cross-section of the studied pHEMT. This general device structure is appropriate for mechanistic research. The TCAD simulation model is also built on this structure, with some modifications according to scanning electron microscope (SEM) observations. The model contains an $Al_{0.3}Ga_{0.7}As/In_{0.25}Ga_{0.75}As$ heterojunction to accumulate the two-dimensional electron gas (2DEG). In the AlGaAs spacer, a δ-doping layer exists to increase the depth of the quantum well. The detailed device parameters are given in Fig. 1. The HPM radiation is equivalent to a sinusoidal interference voltage [26] injected from the gate. The source and drain are set to normal working conditions.

B. NONLINEAR RESPONSE MECHANISM ANALYSIS

Under increasing HPM radiation, the pHEMT's nonlinear transient response (expressed by the output power or drain current) is a "rise – stable – re-rise" process before device burnout. This phenomenon is confirmed by [24] and our experimental results in Section III. The physical mechanism of the nonlinear process is shown in Fig. 2, in which the key device local under HPM radiation is plotted. In the initial "rise" process, the device is operating appropriately since the radiation is relatively weak. Here, we select one random interference cycle to illustrate: the first half $[t_n, t_n + T/2]$ (T is the HPM period) seen in the green part in Fig. 2(a), the condition of the device is shown in Fig. 2(b). In this situation, the output current I_d increases with increasing radiation and can be calculated as

$$I_{d-r} = \frac{WC_0\mu_n}{L}(V_{HPM} - V_t)^2 \tag{1}$$

where L is the gate length, W is the gate width, C_0 is the channel capacitance, and μ_n is the mobility of the 2DEG under a low radiation field. V_t is the threshold voltage, and V_{HPM} is the interference voltage. When the HPM reaches the second half of the cycle, the device is naturally off.

With the enhancement of the microwave radiation, the transient response stabilizes. Similarly, within one random radiation period, the pHEMT's internal states are shown as Fig. 2(b), 2(d) and 2(f) successively, corresponding to the red shaded interference seen in Fig. 2(a), 2(c) and 2(e). Initially, the device operates normally in the saturation region. Then, the interference-driven electric field moves the electrons below the gate upwards, as shown in Fig. 2(d), generating negligible vertical (seen as the y-direction in Fig. 2(b), (d), (f), and (h)) current. For the horizontal (seen as the x-direction in Fig. 2(b), (d), (f), and (h)) component of the interference field is relatively weak, V_d still determines the drain current. As the radiation continues (shown in red in Fig. 2(c) and 2(e)), the horizontal interference field continues to increase, resulting in the pHEMT state changing from Fig. 2(d) to Fig. 2(f). This process includes two steps: a decrease in the negative drain current and an increase in the positive drain current. Moreover, the strong interference field drives a higher vertical current below the gate, which divides the channel current into two opposite parts. After the

reversal of the channel current, the 2DEG drift velocity in the channel reaches saturation. The response current remains constant, which can be calculated as [27]:

$$I_{d-s} = \beta\left(\frac{F_s L}{2}\right)^2 \times \frac{\left[1 + 2\beta R_c V_{HPM'} + \frac{V_{HPM'}^2}{(F_s L/2)^2}\right]^{1/2} - (1 + \beta R_c V_{HPM'})}{1 - \beta^2 R_c^2 (F_s L/2)^2} \tag{2}$$

where $F_s = V_s/2$ is the critical electric field for velocity saturation, R_c is half of the channel resistance, and β is a parameter determined by the device scale. $V_{HPM'} = V_{HPM} - V_t$ reflects the influence induced by the HPM radiation. This analysis indicates that the "stable" of the transient response is attributed to the channel electron velocity saturation under a high horizontal HPM field. The radiation falls back after reaching the peak. The transient response for this duration is considered as a reverse of the former analyzed process: the drain current decreases and returns to its original direction. When the HPM enters the second half, the pHEMT is off, referring to its operating principle.

When facing stronger HPM interference, the transient response rises again after the saturation process [24]. Illustrating one radiation period, when the interference shown as the blue shaded parts in Fig. 2(a), 2(c), 2(e) and 2(g) are injected, the internal states of the pHEMT are shown as Fig. 2(b) – (d) – (f) – (h), respectively. Fig. 2(h) plots the breakdown process in detail. The strong vertical HPM field induces the breakdown below the gate, generating additional current flows into the InGaAs channel. This process includes Au/AlGaAs Schottky junction breakdown and AlGaAs/InGaAs heterojunction breakdown. At the moment of breakdown, the extra current follows the previous flow to the drain. Subsequently, the current changes its direction to the source because it has the lowest potential. Schottky junction breakdown causes extra carrier generation at the gate. The mechanism of this breakdown is a combination of tunneling and impact ionization (II) effects [28]–[31]. The excess tunneling generation rate G_t and II generation rate G_{II} can be calculated utilizing the WKB approximation [32] and the University of Bologna Impact Ionization Model [27], respectively. The breakdown drain current is calculated by:

$$I_{d-re} = -q \int\int Z \cdot \left[f(V_{HPM'}, T)G_t + g(V_{HPM'}, T)G_{II}\right] dxdW \tag{3}$$

where Z is the thickness of the 2DEG. Here, $f(V_{HPM}, T)$ and $g(V_{HPM}, T)$ are the coefficient functions that determine the proportion of two kinds of extra carriers. The mechanism of breakdown explains the secondary ascension of the transient response. As the HPM goes to the second half, the strong reverse electric field quickly depletes the carriers in the channel. Therefore, there is no obvious transient response.

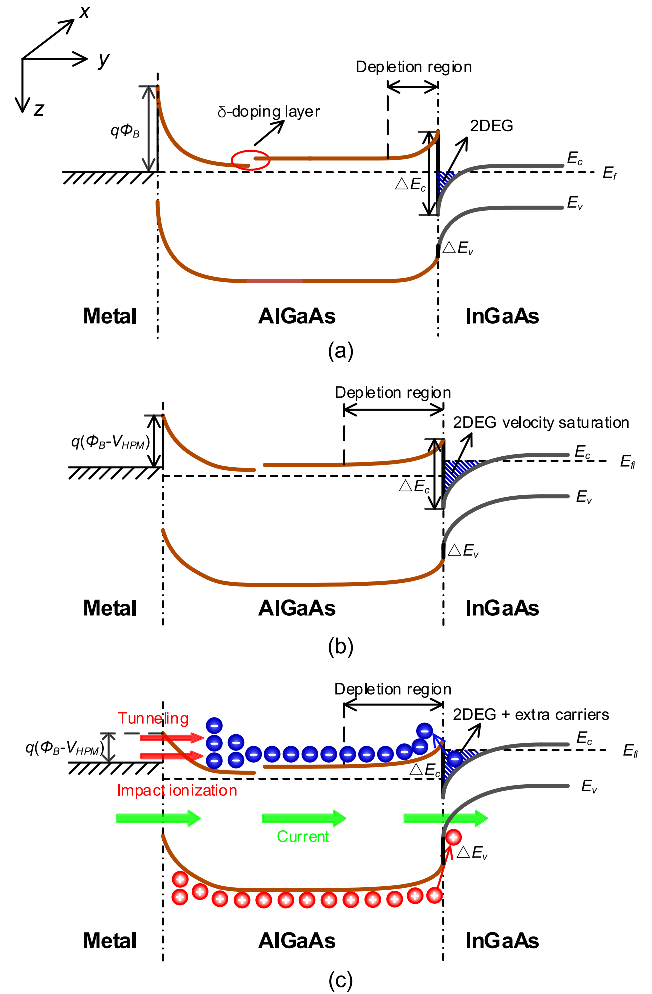

FIGURE 3. Energy band structures of the AlGaAs/GaAs pHEMT under (a) no radiation condition, (b) the electrons velocity saturation condition, (c) the Schottky junction and heterojunction breakdown condition.

Fig. 3 plots the energy band diagrams of the nonlinear response process. With no HPM radiation, the energy band of a zero-biased pHEMT is shown in Fig. 3(a). Here, $q\phi_B$ defines the intrinsic height of the Schottky barrier. The δ-doping layer improves the discontinuity of the conduction band in AlGaAs. A 2DEG is formed and is tightly confined in the InGaAs-side quantum well. As HPM radiation is applied to the device, the energy band changes from Fig. 3(a) to Fig. 3(b): the Schottky barrier drops to $q\ (\phi_B - V_{HPM})$, the Fermi level is lifted in AlGaAs and lowered in InGaAs to Quasi-Fermi levels, ΔE_c is compressed while ΔE_v is expanded in the heterojunction, and the quantum well is deeper, with a higher 2DEG concentration in the channel. When the "stable" transient response is induced by radiation, the energy band is shown in Fig. 3(b). The concentration of the 2DEG reaches saturation under the y-direction interference field, along with the velocity saturation caused by the x-direction HPM field, leading to the "stable" response of the device. The band structure during the "re-rise" process of the nonlinear transient response is shown in Fig. 3(c). In

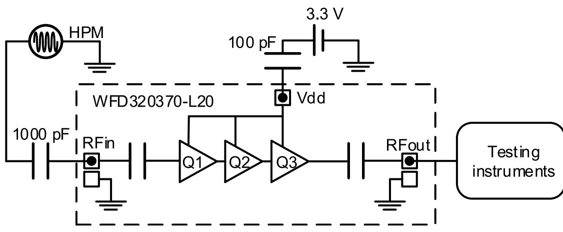

FIGURE 4. Schematic diagram of the testing circuit in the experiment.

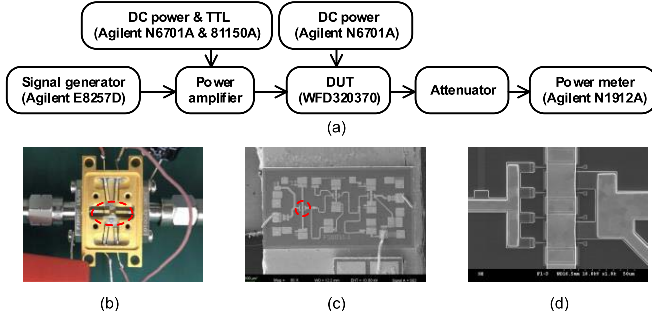

FIGURE 5. (a) The schematic experiment setup. (b) Photograph of the tested chip during the experiments. (c) SEM observation of the three-stage LNA MMIC chip. (d) SEM observation of the first pHEMT in the LNA MMIC chip.

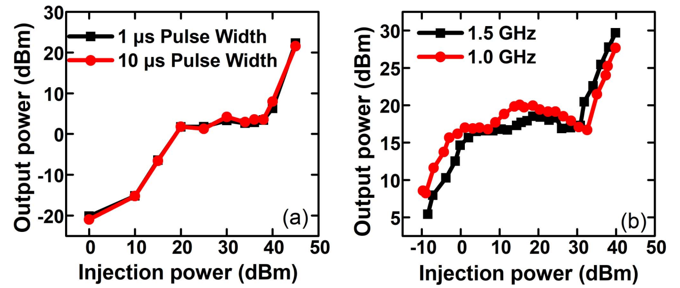

FIGURE 6. (a) The test results under 10-to-50 dBm HPM injection @ 10 GHz with 1 μm and 10 μm pulse widths. (b) The reported test results in [24].

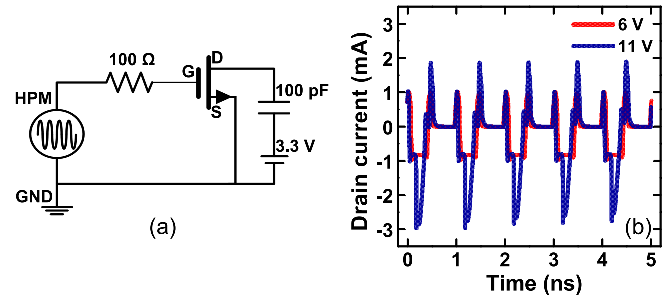

FIGURE 7. (a) Schematic diagram of the HPM simulation circuit. (b) Simulated drain current response from 0 ns to 5 ns under 1 GHz radiation.

addition to the energy band changing further as the trend in Fig. 3(b), extra carriers are generated by the tunneling and impact ionization induced breakdown across the Au/AlGaAs Schottky junction. Then the strong y-direction radiation field drives the extra carriers to cross the heterojunction, resulting in an abnormal current path from the gate to the channel. This explains the "re-rise" of the transient response.

III. RESULTS AND DISCUSSION

A. EXPERIMENTAL SETUP AND RESULTS

Corresponding experiments are implemented to verify the mechanism. The device under test (DUT) is a WFD320370-L20 GaAs pHEMT Ka-band LNA MMIC chip. Fig. 4 shows the simplified schematic diagram of the testing circuit used in the HPM experiments. The chip is biased to its general working state @ $V_{dd} = 3.3$ V. The HPM interference injections are from 0 dBm to 50 dBm @ 10 GHz, with pulse widths of 1 μs and 10 μs. The experimental setup and the microanalysis of the DUT are given in Fig. 5, and the SEM shows the surface morphology in detail.

Fig. 6(a) exhibits the experimental results for the nonlinear transient response. The output power shows a "rise – stable – re-rise" tendency, which is consistent with the mechanism analysis. Moreover, the pulse width has little influence on the nonlinear response under these test conditions. For further confirmation, similar test results with different interference frequencies reported in [24] are shown in Fig. 6(b).

B. SIMULATION VERIFICATION AND DISCUSSION

Hydrodynamic, high-field saturation, Auger, avalanche, barrier tunneling, and thermodynamic models are utilized in TCAD for more accurate simulations [25]. The testing circuit used in the simulation is shown in Fig. 7(a), which indicates good agreement with the experiments. Simulation results from 0 ns to 5 ns are plotted in Fig. 7(b), and the HPM frequency is fixed at 1 GHz. Under different radiation levels (with 6 V and 11 V selected as examples), the transient response I_d shows a periodic tendency. A detailed response (with 10 ns to 12 ns selected as examples) is plotted in Fig. 8. The "rise" process of the nonlinear response is observed in Fig. 8(a), the drain current rises with the increase of the radiation. Then, the "stable" process is shown in Fig. 8(b); as the radiation increases from 6 V to 8 V, the response current remains unchanged. Fig. 8(c) plots the "re-rise" process. The breakdown happens when there is a sudden surge in the drain current. Subsequently, the current continues to increase until the interference field declines. Moreover, the drain current changes its orientation (I_d changes its positive and negative) twice each radiation period in every stage of the nonlinear response process. The simulation results are in good consistency with the experiments and theoretical analysis above.

Fig. 9(a) and (b) present the current density distribution inside the device at 11 ns (point A in Fig. 8(b)) and 11.25 ns (point B in Fig. 8(b)) under 6 V interference. It can be seen that the drain current changes its direction and approaches saturation. For the breakdown process, the internal states of the device under 13 V interference at points C (11.15 ns) and D (11.35 ns) in Fig. 8(c) are plotted in Fig. 9(c) and (d). The simulations imply that the "two-part" channel remains at the

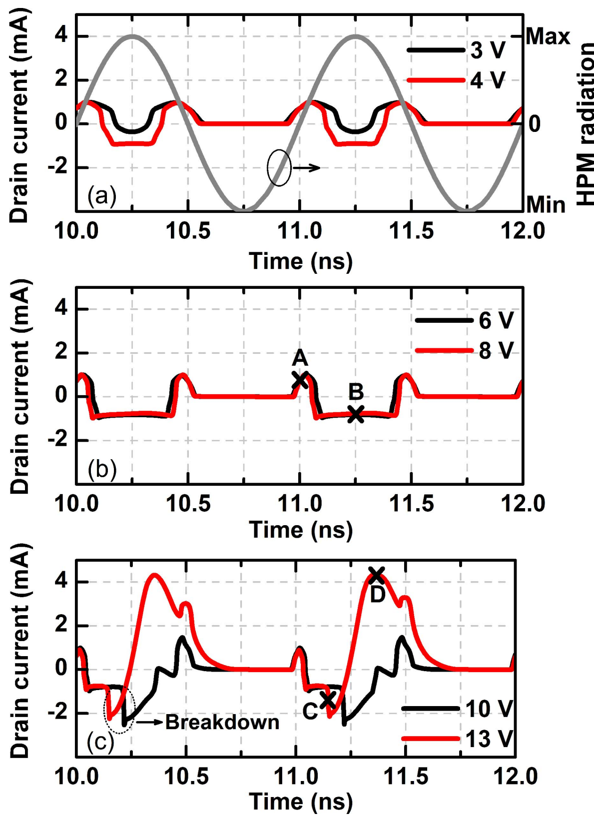

FIGURE 8. Simulated drain current response from 10 ns to 12 ns under (a) 2 V to 3 V, (b) 6 V to 8 V, (c) 10 V to 13 V HPM radiation; the frequency is 1 GHz as shown as (a).

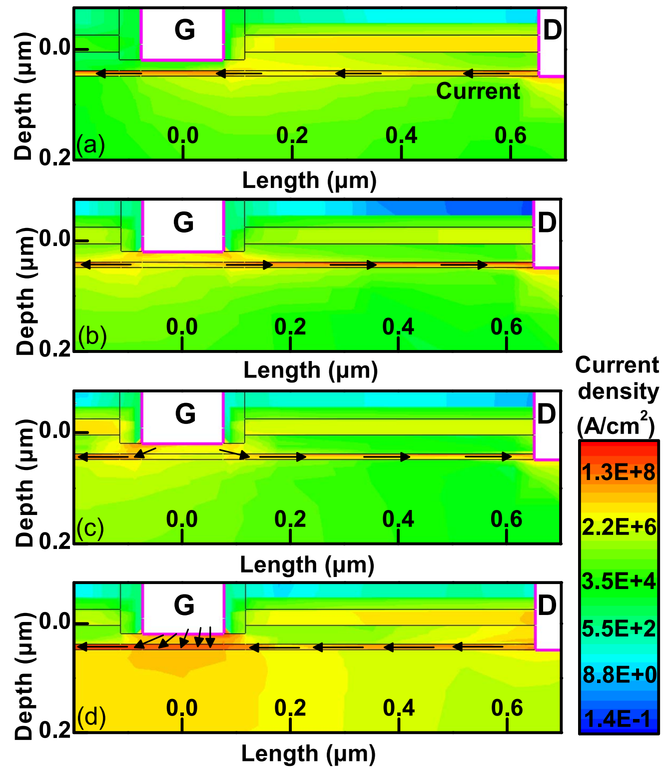

FIGURE 9. The current density distribution of the pHEMT at (a) 11 ns under 6 V HPM, (b) 11.25 ns under 6 V HPM, (c) 11.15 ns under 13 V HPM, and (d) 11.35 ns under 13 V HPM.

beginning of the breakdown. Then, a significant additional current is injected into the channel and eventually flows to the source, which is consistent with the mechanism analysis.

Fig. 10 shows the simulated transient output power of the AlGaAs/InGaAs pHEMT under HPM radiation with different frequencies. A “rise – stable – re-rise” nonlinear response can be found. The output power drops slightly with increasing frequency. Moreover, the knee points in the simulations are reached earlier than in the experiments. This is caused by the packaging and peripheral circuit differences between the simulation and actual ICs.

The phenomenon of nonlinear transient response can bring different disturbances to the RF front-end circuits. Here we use pHEMT-based LNAs to explain. In the first “rise” condition, the HPM is regarded as noise and is amplified together with the useful signal. Therefore, there is an output signal distortion in the LNA, and the output signal-to-noise ratio (SNR) decreases significantly. As the transient response of the device enters into the “stable” status, the LNA loses the function of signal amplification. Furthermore, the gain of the LNA drops as I_g continues to increase. The breakdown occurs when the “re-rise” of the drain current is observed. The HPM power is transmitted straight to the next level of the circuit, resulting in more negative effects. Knowing our mechanism analysis to the nonlinear transient

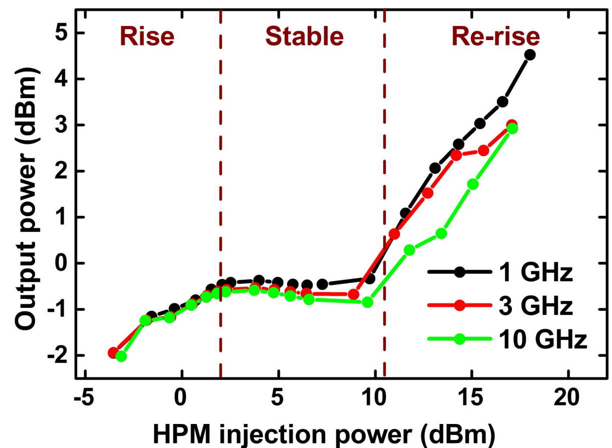

FIGURE 10. Simulation results of pHEMT’s output power under 1-to-10 GHz HPM radiation.

response process, targeted solutions are used to deal with the circuit disorders. The “rise” process upset is an over-noise upset, which can be mitigated by using pHEMTs with better performance and shielding the transmission line between the LNA and the antenna [33]. In contrast, the “stable” and “re-rise” process disturbances are overpower disturbances, and adding a limiter at the LNA input is a feasible solution [34]–[36]. Moreover, if the “re-rise” process is observed in circuits, the LNA should be diagnosed as a

failure because the breakdown is unrecoverable in a short time.

IV. CONCLUSION

This study has discussed the physical mechanism of the HPM induced nonlinear response in AlGaAs/InGaAs pHEMT. We view the phenomenon as a "rise – stable – re-rise"İ process. During the first "rise" stage, the pHEMT functions normally. The following "stable" is due to the electron velocity saturation in the channel. Lastly, the HPM field breaks the Schottky gate and the heterojunction under the mechanisms of tunneling and impact ionization, generates an extra current path to the channel. This abnormal current causes the "re-rise" of the pHEMT's transient response. TCAD simulations confirm these physical processes. Experiments are carried out using a GaAs-based Ka-band LNA chip to support our analysis. This paper has provided a deeper insight into the HPM radiation reliability of the pHEMT. In future investigations, it might be possible to have a device-level hardening design based on this study.

REFERENCES

[1] J. A. del Alamo, "Nanometre-scale electronics with III–V compound semiconductors," *Nature*, vol. 479, no. 7373, pp. 317–323, Nov. 2001.

[2] D.-H. Kim *et al.*, "High-performance III–V devices for future logic applications," in *Proc. 60th IEEE Int. Electron Device*, San Francisco, CA, USA, Dec. 2014, pp. 578–581.

[3] J. A. del Alamo, D. A. Antoniadis, J. Lin, W. Lu, A. Vardi, and X. Zhao, "Nanometer-scale III-V MOSFETs," *IEEE J. Electron Device Soc.*, vol. 4, no. 5, pp. 205–214, Sep. 2016.

[4] E. Lind, E. Memišević, A. W. Dey, and L.-E. Wernersson, "III-V heterostructure nanowire tunnel FETs," *IEEE J. Electron Device Soc.*, vol. 3, no. 3, pp. 96–102, May 2015.

[5] J. Ajayan and D. Nirmal, "20-nm enhancement-mode metamorphic GaAs HEMT with highly doped InGaAs source/drain regions for high-frequency applications," *Int. J. Electron.*, vol. 104, no. 3, pp. 504–512, Mar. 2017.

[6] T. Kosugi *et al.*, "A 125-GHz 140-mW InGaAs/InP composite-channel HEMT MMIC power amplifier module," *IEICE Electron. Exp.*, vol. 6, no. 24, pp. 1764–1768, Dec. 2009.

[7] K. C. Hwang *et al.*, "Very high gain millimeter-wave InAlAs/InGaAs/GaAs metamorphic HEMT's," *IEEE Electron Device Lett.*, vol. 20, no. 11, pp. 551–553, Nov. 1999.

[8] Y.-C. Lin, E. Y. Chang, H. Yamaguchi, W.-C. Wu, and C.-Y. Chang, "A δ-doped InGaP/InGaAs pHEMT with different doping profiles for device-linearity improvement," *IEEE Trans. Electron Devices*, vol. 54, no. 7, pp. 1617–1625, Jul. 2007.

[9] W. A. Radasky, C. E. Baum, and M. W. Wik, "Introduction to the special issue on high-power electromagnetics (HPEM) and intentional electromagnetic interference (IEMI)," *IEEE Trans. Electromagn. Compat.*, vol. 46, no. 3, pp. 314–321, Aug. 2014.

[10] D. Nitsch, M. Camp, F. Sabath, J. L. T. Haseborg, and H. Garbe, "Susceptibility of some electronic equipment to HPEM threats," *IEEE Trans. Electromagn. Compat.*, vol. 46, no. 3, pp. 380–389, Aug. 2004.

[11] M. Camp, H. Gerth, H. Garbe, and H. Haase, "Predicting the breakdown behavior of microcontrollers under EMP/UWB impact using a statistical analysis," *IEEE Trans. Electromagn. Compat.*, vol. 46, no. 3, pp. 368–379, Aug. 2004.

[12] J. W. Chung, W. E. Hoke, E. M. Chumbes, and T. Palacios, "AlGaN/GaN HEMT with 300-GHz f_{max}," *IEEE Electron Device Lett.*, vol. 31, no. 3, pp. 195–197, Mar. 2010.

[13] Z. Tang *et al.*, "600-V normally off SiN_x/AlGaN/GaN MIS-HEMT with large gate swing and low current collapse," *IEEE Electron Device Lett.*, vol. 34, no. 11, pp. 1373–1375, Nov. 2013.

[14] K. M. K. H. Leong *et al.*, "A 0.85 THz low noise amplifier using InP HEMT transistors," *IEEE Microw. Wireless Compon. Lett.*, vol. 25, no. 6, pp. 397–399, Jun. 2015.

[15] X. Huang, Z. Liu, Q. Li, and F. C. Lee, "Evaluation and application of 600 V GaN HEMT in cascode structure," *IEEE Trans. Power Electron.*, vol. 29, no. 5, pp. 2453–2461, May 2014.

[16] W. Wang *et al.*, "Improvement of power performance of GaN HEMT by using quaternary InAlGaN barrier," *IEEE J. Electron Devices Soc.*, vol. 6, pp. 360–364, Feb. 2018. [Online]. Available: https://ieeexplore.ieee.org/document/8293769

[17] S. A. Ahsan, S. Ghosh, S. Khandelwal, and Y. S. Chauhan, "Physics-based multi-bias RF large-signal GaN HEMT modeling and parameter extraction flow," *IEEE J. Electron Device Soc.*, vol. 5, no. 5, pp. 310–319, Sep. 2017.

[18] D. S. James and L. Dormer, "A study of high power pulsed characteristics of low-noise GaAs MESFETs," in *IEEE MTT-S Int. Microw. Symp. Dig.*, Los Angeles, CA, USA, Dec. 1981, pp. 1298–1310.

[19] C. Zhang, H. Wang, J. Zhang, G. Du, and J. Yang, "Failure analysis on damaged GaAs HEMT MMIC caused by microwave pulse," *IEEE Trans. Electromagn. Compat.*, vol. 56, no. 6, pp. 1545–1549, Dec. 2014.

[20] L. Zhou *et al.*, "Investigation on failure mechanisms of GaN HEMT caused by high-power microwave (HPM) pulses," *IEEE Trans. Electromagn. Compat.*, vol. 59, no. 3, pp. 902–909, Jun. 2017.

[21] J. Xu, W.-Y. Yin, J.-F. Mao, and L.-W. J. Li, "Thermal transient response of GaAs FETs under intentional electromagnetic interference (IEMI)," *IEEE Trans. Electromagn. Compat.*, vol. 50, no. 5, pp. 340–346, May 2008.

[22] L. Yang, C.-C. Chai, Y.-T. Yang, J. Sun, and Z.-P. Li, "Damage effect and mechanism of the GaAs high electron mobility transistor induced by high power microwave," *Chin. Phys. B*, vol. 25, no. 4, Apr. 2016, Art. no. 048504.

[23] P. Xue, J. Fang, Z. Li, and J. Sun, "Simulation study of high power microwave damage effect on GaAs HEMT," in *Proc. 11th Int. Symp. Antennas Propag. EM Theory*, Guilin, China, Oct. 2016, pp. 636–639.

[24] C. Zhang, H. Wang, J. Zhang, and G. Du, "Experiment and simulation of the nonlinear and transient responses of GaAs PHEMT injected with microwave pulses," *IEEE Trans. Electromagn. Compat.*, vol. 57, no. 5, pp. 1132–1138, Oct. 2015.

[25] *Sentaurus Device User Guide Version L-2016.03*, Synopsys, San Jose, CA, USA, Mar. 2016, p. 427.

[26] S. Korte, M. Camp, and H. Garbe, "Hardware and software simulation of transient pulse impact on integrated circuits," in *Proc. IEEE Int. Symp. Electromagn. Compat.*, Chicago, IL, USA, Aug. 2005, pp. 489–494.

[27] K. Lee, M. S. Shur, T. J. Drummond, and H. Morkoc, "Current–voltage and capacitance–voltage characteristics of modulation-doped field-effect transistors," *IEEE Trans. Electron Devices*, vol. 30, no. 3, pp. 207–212, Mar. 1983.

[28] R. J. Trew and U. K. Mishra, "Gate breakdown in MESFETs and HEMTs," *IEEE Electron Device Lett.*, vol. 12, no. 10, pp. 524–526, Oct. 1991.

[29] M. H. Somerville, C. S. Putnam, and J. A. del Alamo, "Determining dominant breakdown mechanisms in InP HEMTs," *IEEE Electron Device Lett.*, vol. 22, no. 12, pp. 565–567, Dec. 2001.

[30] S. R. Bahl and J. A. del Alamo, "Physics of breakdown in InAlAs/n^+-InGaAs heterostructure field-effect transistors," *IEEE Trans. Electron Devices*, vol. 41, no. 12, pp. 2268–2275, Dec. 1994.

[31] S. Takamiya *et al.*, "Reverse currents of schottky gates of III–V MESFET/HEMTs: Field emission and tunnel currents," *Solid-State Electron.*, vol. 42, no. 3, pp. 447–451, Mar. 1998.

[32] H. P. Li, O. L. Hartin, and M. Ray, "An updated temperature-dependent breakdown coupling model including both impact ionization and tunneling mechanisms for AlGaAs/InGaAs HEMTs," *IEEE Trans. Electron Devices*, vol. 49, no. 9, pp. 1675–1678, Sep. 2002.

[33] S. D. Nsele *et al.*, "Ka-band low noise amplifiers based on InAlN/GaN technologies," *presented at the IEEE Int. Conf. Noise Fluctuations (ICNF)*, Xian, China, Jun. 2015, pp. 1–4.

[34] J. Chenyang and P. Longxin, "Design of Ka band MMIC limiter low noise amplifier," presented at the Int. Conf. Comput. Sci. Inf. Technol. (ICCSIT), Daqing, China, Dec. 2018, Art. no. 022040.

[35] L. Pantoli *et al.*, "Gallium arsenide 0.5–18 GHz antenna front-end with integrated limiter and differential to single ended low-noise amplifier," *IET Microw. Antennas Propag.*, vol. 12, no. 6, pp. 947–953, May 2018.

[36] P. Mahmoudidaryan and A. Medi, "Codesign of Ka-Band integrated limiter and low noise amplifier," *IEEE Trans. Microw. Theory Techn.*, vol. 64, no. 9, pp. 2843–2852, Sep. 2016.

YU-QIAN LIU received the B.S. degree from the School of Physics and Optoelectronic Engineering, Xidian University, Xi'an, China, in 2011, where he is currently pursuing the Ph.D. degree in microelectronics and solid-state electronics with the School of Microelectronics. His research interests include the HPM reliability and interference mechanism of III-V compound semiconductor, EMP effect, and mechanism of CMOS logic circuits.

CHANG-CHUN CHAI received the B.S. degree in microelectronics and solid-state electronics from Tsinghua University, Beijing, China, in 1982, and the M.S. degree in microelectronics and solid-state electronics and the Ph.D. degree in electronic science and technology from Xidian University, Xi'an, China, in 1990 and 2005, respectively.

He has been a Professor with the School of Microelectronics, Xidian University, since 2001. His research interests include the semiconductor devices and reliability of integrated circuits, semiconductor devices technology, and integrated circuits design.

HAN WU received the B.S. degree from the School of Microelectronics, Xidian University, in 2012. He is currently pursuing the Ph.D. degree in microelectronics and solid-state electronics. His research interests include the HPM reliability design of RF circuits.

YU-HANG ZHANG received the B.S. and M.S. degrees in microelectronics from Xidian University, Xi'an, China. He is currently pursuing the Ph.D. degree with the Department of Micro-Nano Electronics, Shanghai Jiao Tong University, Shanghai, China. His research interests include design and reliability of SRAMs and RF circuits.

CHUN-LEI SHI received B.S. degree in microelectronics from Xidian University, Xi'an, China, in 2008. She is a Lecturer with China Civil Aviation University, Tianjin, China. Her current research interests include electromagnetic-compatibility-related analysis of printed circuit boards and ICs, reliability of integrated circuits, and semiconductor devices.

YIN-TANG YANG (Senior Member, IEEE) received the B.S., M.S., and Ph.D. degrees in microelectronics from Xidian University, Xi'an, China.

He is currently the Vice-President of Xidian University and a Professor and the Ph.D. Director of integrated circuit design, very large scale integration, and microelectronics with Xidian University. His current research interests include high-speed data converters, 3-D integrated circuits, network-on-a-chip, and new semiconductor devices.